Hindawi
Advances in Civil Engineering
Volume 2024, Article ID 1672269, 14 pages
https://doi.org/10.1155/2024/1672269

Research Article

Conservativeness Study on the Seismic Analysis Method for Research Reactor Plant Structure Based on TMSR-LF1

Rencong Dai,[1,2] **Wei Gong**,[1] **Xiao Wang**,[1] **Xiaoyan Wang**,[1] **and Decheng Cui**[1]

[1]*Shanghai Institute of Applied Physics, Chinese Academy of Sciences, Shanghai 201800, China*
[2]*University of Chinese Academy of Sciences, Beijing 100049, China*

Correspondence should be addressed to Wei Gong; gongwei@sinap.ac.cn and Xiao Wang; wangxiao@sinap.ac.cn

Received 23 August 2023; Revised 24 October 2023; Accepted 17 January 2024; Published 31 January 2024

Academic Editor: Emanuele Brunesi

The seismic performance analysis of research reactor plants is crucial for ensuring the safety of the entire reactor system. This paper analyzes the plant structure seismic performance of the 2WMt Thorium Molten Salt Reactor-Liquid Fuel 1 (TMSR-LF1) at the Shanghai Institute of Applied Physics, Chinese Academy of Sciences under the action of frequent earthquakes, fortification earthquakes, and rare earthquakes was analyzed by finite element software PKPM based on the seismic design method of civil code +1°. On this basis, a comparison was made between the seismic responses of structural pushover analysis and elastoplastic time history analysis under the action of rare earthquakes, and the conservatism of these two commonly used methods for elastoplastic analysis was systematically analyzed. The results indicate that the TMSR-LF1 plant structure exhibits well bearing and deformation capacity. It meets the seismic design goal of "no damage under small earthquakes," "no unrepairable damage under medium earthquakes," and "no collapse under large earthquakes (using static pushover analysis)," and the critical regions are entirely within the elastic range. Furthermore, the analysis reveals that the elastoplastic time history analysis method produced a significantly higher seismic response than the pushover analysis method, which indicates the conservativeness of the time history method. Therefore, it is recommended to use the elastoplastic time history analysis method to evaluate the seismic performance of research reactor plants under rare earthquake actions. The research in this paper provides important references for the seismic performance analysis of other Class II research reactor plants.

1. Introduction

The research reactor plant plays a crucial role in exploring advanced nuclear power technologies and contributes significantly to the achievement of sustainable development goals. Compared with nuclear power reactors, research reactors are characterized by lower power output and a reduced risk of radioactive product release. According to the National Nuclear Safety Administration (NNSA), research reactors are classified into three categories based on the potential risks they pose: Class I, Class II, and Class III [1, 2]. The 2WMt Thorium Molten Salt Reactor-Liquid Fuel 1 (TMSR-LF1), currently under construction in Gansu Province, China, belongs to the Class II research reactor as classified by the NNSA [3–6].

The seismic performance analysis of nuclear reactor plants is crucial for ensuring the entire system's safety. The primary focus is on solving nonlinear equations in seismic analysis. Numerous scholars have extensively researched the solution of nonlinear equations in vibration analysis, exploring both analytical and numerical methods. While the analytical method offers high computational accuracy, it often involves complex calculations, which makes it impractical for complex physical systems [7–9]. On the other hand, the numerical method relies on numerical computation to obtain simulation results for complex systems without the need for complicated mathematical formulas. Therefore, it is better suited for engineering applications. Current research on the seismic performance of nuclear power plants mainly revolves around utilizing two primary numerical analysis methods: the pushover analysis (static elastoplastic analysis) and the elastoplastic time history analysis (dynamic elastoplastic analysis) method. The pushover analysis is an efficient method that can provide a structure's seismic performance quickly, as seen in the study conducted by Xue et al. [10] on the containment

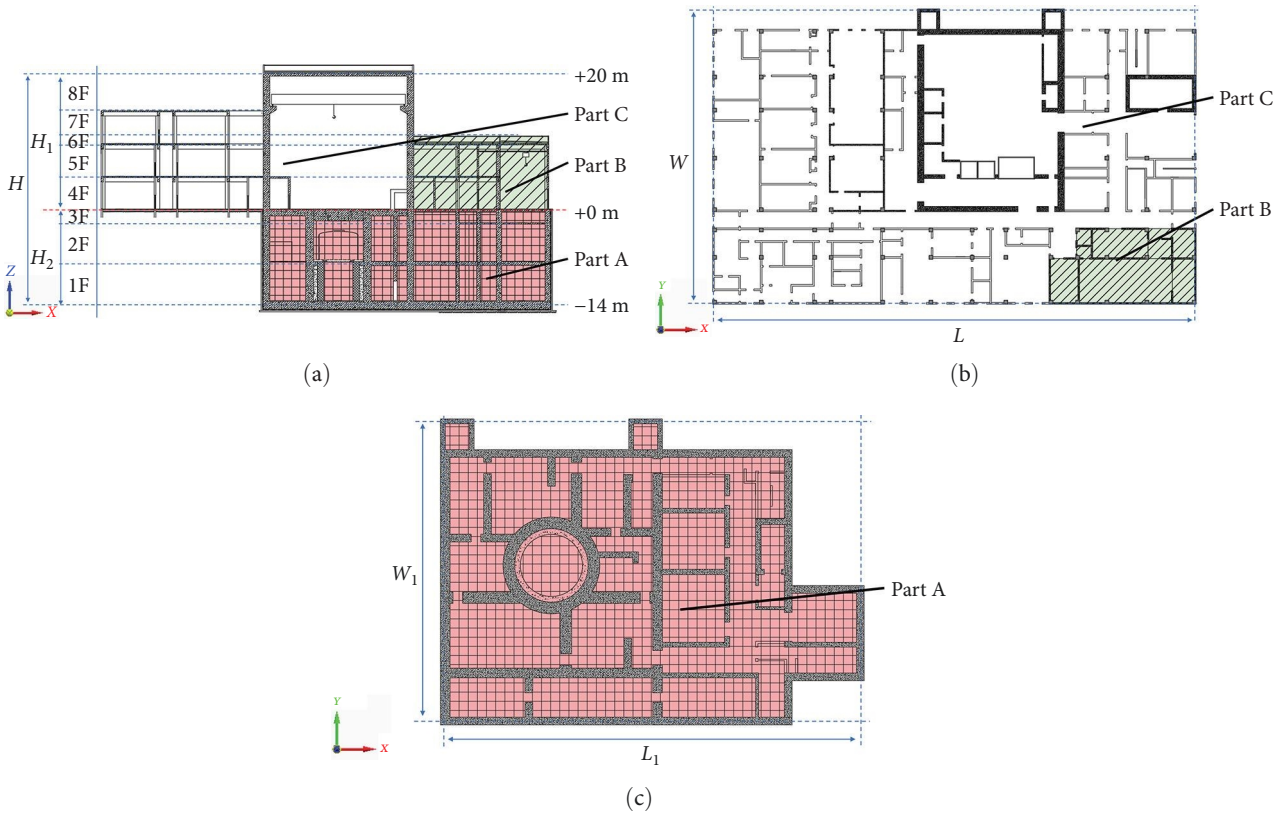

Figure 1: The sketch and zoning of TMSR-LF1 structure: (a) elevation view; (b) +0 m floor plan; (c) −14 m floor plan.

structure of a nuclear power plant, while Qi and Wan [11] and Zhao et al. [12] also utilized this method to investigate the seismic performance of nuclear power plant buildings under different earthquake conditions. Pan et al. [13] utilized the pushover analysis to examine the seismic performance characteristics of safety-related structures in typical nuclear power plants during the excess design basis earthquake, while Zhao and Zhang [14] applied it to a nuclear power plant's radioactive solid waste plant to evaluate the component damage of the structure under different levels of seismic activity. The time history analysis method was once less commonly used due to its time-consuming nature, but recent developments in computer technology have increased its accuracy and efficiency, leading to an increase in its utilization. Wang et al. [15, 16] used both the pushover analysis and the elastoplastic time history analysis methods to study the seismic performance of nuclear power plant containment. Their study focused on the stiffness and seismic response of the structure under ultimate safety earthquake (SL-2). Farmanbordar et al. [17] also employed two elastoplastic analysis methods to investigate the seismic performance of a base-isolated nuclear power plant and the impact of different seismic isolation bearing types.

Despite extensive research on the seismic performance of nuclear reactor plants, some limitations still exist. Most studies have concentrated on nuclear power reactor plants, with relatively fewer investigations conducted on research reactor plants. Furthermore, several researchers have utilized different seismic analysis methods, yet there is a lack of studies that systematically compare the conservativeness of the pushover analysis and the elastoplastic time history analysis. In this paper, the seismic design method of civil code +1° [18–20] was utilized with the finite element software PKPM [21] to analyze the seismic performance of the TMSR-LF1 plant structure. The study evaluated the seismic behavior of the plant structure by systematically investigating its elastic and elastoplastic response under frequent earthquakes (50-year exceedance probability of 63% ground motions, i.e., small earthquakes), fortification earthquakes (50-year exceedance probability of 10% ground motions, i.e., medium earthquakes), and rare earthquakes (50-year exceedance probability of 2%–3% ground motions, i.e., large earthquakes). On this basis, the structural response results of the pushover analysis and the elastoplastic time history analysis were compared, and the conservativeness of the two analysis methods was comprehensively analyzed. These research results could provide a valuable reference for seismic performance analysis of the Class II research reactor building in the future.

2. Computation Model

2.1. Structural Model. The overall structure of the TMSR-LF1 nuclear plant is sketched in Figure 1, and its horizontal and vertical direction are described by L (76.1 m), W (43.2 m), and H (34.0 m). The length, width, and height of the model correspond to the X, Y, and Z directions in Figure 1, respectively. The plant could be divided into aboveground and underground parts (bounded by +0 m elevation), with the

Table 1: The height and floor elevation of each floor of TMSR-LF1.

Floor	Floor height (m)	Base plate elevation (m)	Top plate elevation (m)
8	5	+15	+20
7	3	+12	+15
6	2	+10	+12
5	5	+5	+10
4	5	+0	+5
3	2	−2	+0
2	6	−8	−2
1	6	−14	−8

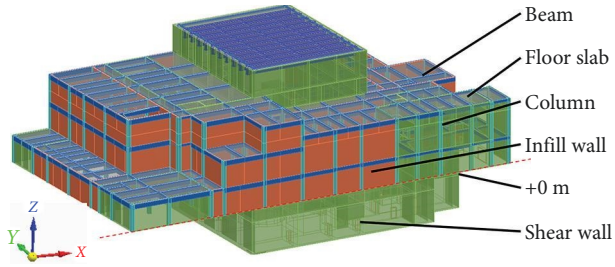

Figure 2: The 3D model of TMSR-LF1.

Table 2: The floor distribution and component information of TMSR-LF1.

Part	Floor	Thickness and section dimensions (mm)				
		Shear wall	Floor slab	Beam	Column	Infill wall
A	1–3	800–1,200	200–1,800	—	—	—
B	4–6	240	150–200	400 × (600–700)	600 × 600	—
C	4–8	200–1,000	150–200	400 × (450–900)	600 × 600	240

aboveground part having the same dimensions as the overall structure, except for the height H_1 (20.0 m). The underground part has smaller dimensions with length, width, and height indicated by L_1 (44.1 m), W_1 (31.2 m), and H_2 (14.0 m), respectively. The plant consists of eight floors, five of which are aboveground and three are underground. The height and elevation of each floor slab are shown in Table 1.

The TMSR-LF1 plant is a typical reinforced concrete frame-shear wall structure that comprises beams, columns, shear walls, infill walls, and floor slabs. The beams, columns, shear walls, and floor slabs are made of reinforced concrete casting, which mainly plays the role of side force resistance and load bearing. While the infill walls are constructed of concrete bricks, and the main difference with the above is that it does not contain reinforcing materials, and only plays the role of enclosure and separation. The 3D solid model of the TMSR-LF1 plant is shown in Figure 2.

The TMSR-LF1 can also be divided into three parts, denoted A, B, and C, according to the significance of the systems and equipment (as shown in Figure 1). The details of floor distribution, components, and dimensions of each part are provided in Table 2. Part A comprises the whole underground area (1F–3F), which is the core area of the plant, including the reactor system, the reactor surround system, and the related auxiliary equipment rooms. This section comprises thick shear walls (thickness of 800–1,200 mm) and floor slabs (maximum thickness of 1,800 mm). Part B is in the southeastern part of the plant (4F–6F) and encompasses the main reaction room for salt addition mixing, the control room for salt addition mixing, and the fuel pretreatment room for salt addition mixing tail gas treatment. This section consists of floor slabs, beams, columns, and medium-thick shear walls (240 mm thick). Part C is situated in the remaining aboveground part of the plant (four to eight floors), including working rooms such as stacking halls, distribution rooms, and maintenance rooms. The main difference between Part B is that its wall elements are made up of infill walls with a thickness of 240 mm and a small number of thicker but larger span (maximum span is 28.6 m) shear walls. Based on the aforementioned information, it is evident that the structural stiffness of Part A for the TMSR-LF1 plant is the largest, followed by Part B, and Part C has the lowest structural stiffness.

2.2. Finite Element Model. The finite element modeling of the TMSR-LF1 plant was modeled using the 3D finite element software PKPM developed by the China Academy of Building Research. Due to the complex configuration and distribution of the TMSR-LF1 plant, it is necessary to simplify the treatment

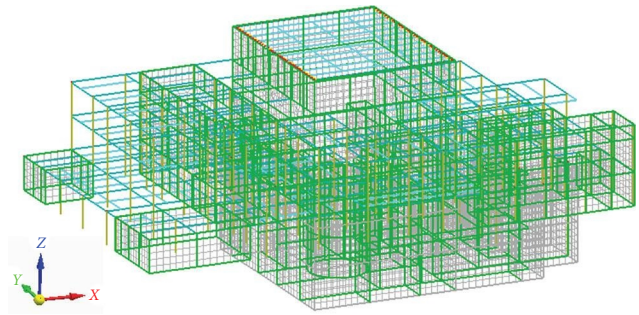

Figure 3: The finite element model of TMSR-LF1.

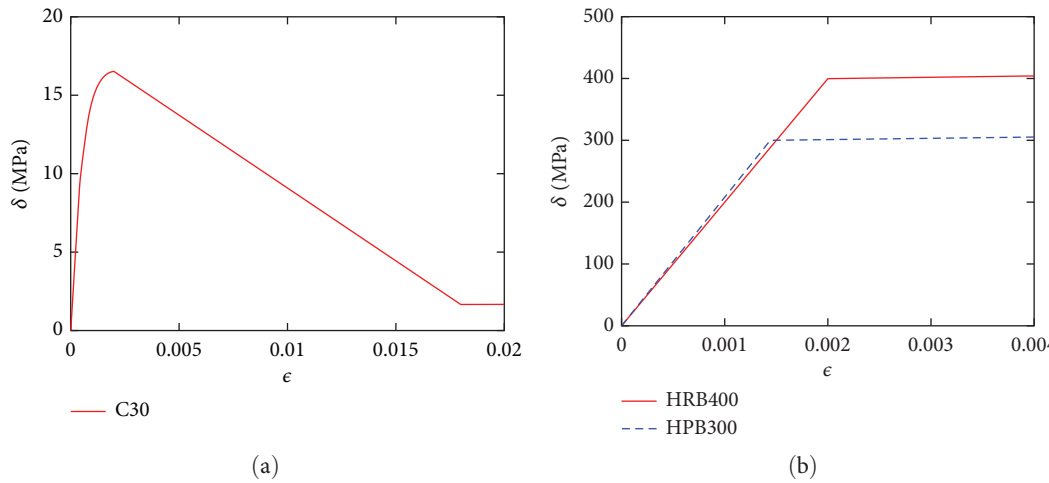

Figure 4: Constitutive relations of the materials: (a) constitutive relation of C30; (b) constitutive relation of HRB400 and HPB300.

during calculation. First, infill walls were converted into regular mass loads as the system equipment and applied to the corresponding beams and floor slabs. Since this simplification results in losing some structural stiffness, the period reduction factor was set to 0.8 to supplement the structural stiffness [22]. The beams and columns were simplified to 1D linear beam elements, and the shear walls and floor slabs were simplified to 2D shell elements. Additionally, the lateral restraint effect of the considered foundation soil on the plant basement was simplified using the additional stiffness [23], which was calculated as shown in Equation (1). The sketch of the simplified 3D finite element model of TMSR-LF1 is shown in Figure 3.

$$K = 1,000 \times m \times H\ , \tag{1}$$

where K is the additional stiffness; m is the scale factor of the horizontal resistance coefficient of the foundation soil, which is taken as 6.0 in this paper; H is the burial depth.

The structural finite element model includes concrete and reinforcing steel materials, while their constitutive relationship curves are shown in Figure 4. Concrete material with a strength grade of C30 is modeled using SAENZ curves [24] for the ascending segment of its constitutive relationship, while straight lines are used for the other segments (Figure 4(a)); HRB400 and HPB300 are used for the steel bar, and its constitutive relationship is characterized by a bilinear model with a slope ratio of 0.01 (Figure 4(b)).

2.3. Analysis Method. The structural seismic analysis methods used in this paper include response spectrum analysis, pushover analysis, and elastoplastic time history analysis methods.

2.3.1. Response Spectrum Analysis Method. The response spectrum analysis [25] is a seismic analysis method based on the vibration decomposition reaction spectrum theory, which is mainly characterized by high computational efficiency and accurate calculation results. Characterized by high computational efficiency and accurate results, it was used in this study for the elastic calculation of TMSR-LF1 subjected to frequent earthquakes and fortification earthquakes. The calculation formula for multidegrees of freedom is shown in Equation (2).

$$F_{ji} = \left(G_i \alpha_j \gamma_j \varphi_{ji}\right)\ , \tag{2}$$

where F_{ji} is the horizontal seismic force of mass i at the jth vibration mode; G_i is the weight of mass i, α_j is the jth vibration type seismic influence coefficient calculated by the jth order period of the system, γ_j is the vibration type participation coefficient, φ_{ji} is the value of the jth vibration type at the ith mass.

Table 3: The parameters of the input ground motion of TMSR-LF1.

Parameters	Frequent earthquakes	Fortification earthquakes	Rare earthquakes
PGA (g)	0.09	0.27	0.46
Horizontal earthquake effect coefficient	0.23	0.70	1.35

Table 4: The values of the EDP of TMSR-LF1.

EDP	Frequent earthquakes	Fortification earthquakes	Rare earthquakes
Story drift ratio ($\times 10^{-3}$ rad)	1.25	2.50	10.00

2.3.2. Pushover Analysis Method. The pushover analysis [26] is an efficient and convenient elastoplastic analysis method based on structural statics and elastoplastic theory. Hence, it was adopted for the elastoplastic calculation of TMSR-LF1 under rare earthquakes in this paper. The main calculation equations are as follows:

$$\begin{cases} S_{a1} = (V/G)/\alpha_1 \\ S_{d1} = \Delta T_1/\gamma_1 \varnothing_{1,T} \end{cases}, \tag{3}$$

$$S_{d2} = T_2^2 S_{a2} g/4\pi^2 , \tag{4}$$

where S_{a1} and S_{a2} are the acceleration values of the capability spectrum and demand spectrum, respectively; S_{d1} and S_{d2} are the displacement values of capability spectrum and demand spectrum, respectively; T_1 and T_2 are the period values of capability spectrum and demand spectrum, respectively; γ_1, α_1, and $\varnothing_{1,T}$ are the first vibration type participation coefficient, mass participation coefficient and vertex amplitude, respectively; V is the base shear value; G is the representative value of total load effect; g is the gravitational acceleration.

2.3.3. Elastoplastic Time History Analysis Method. The elastoplastic time analysis [27] is an accurate elastoplastic analysis method based on structural dynamics and elastoplastic theory. This method is notable for its high computational accuracy and ability to provide a more realistic seismic response to complex structures. Considering the complex structure of the TMSR-LF1 plant, this method was also used to calculate the elastoplastic response of the structure under rare earthquakes. The kinetic expressions are shown in Equation (5).

$$M\ddot{u} + C\dot{u} + Ku = -M\ddot{u}_g , \tag{5}$$

where M, C, and K are the matrices of mass, damping, and stiffness of the vibration system, respectively; $\ddot{u}$, $\dot{u}$, and u are the acceleration, velocity, and displacement of the nodes, respectively; and $\ddot{u}_g$ is the ground motion acceleration.

2.4. Seismic Analysis Parameters. The method of civil code +1° was employed in the seismic design of the TMSR-LF1 plant. According to the investigation and measurement on the site of TMSR-LF1 by the China Earthquake Administration [28], the seismic fortification intensity of the site is 7°; thus, the seismic fortification intensity was set to 8° in the seismic analysis. The peak ground acceleration (PGA), as a widely utilized ground motion intensity [29–31], is adopted as the intensity index in this paper. The maximum value of the horizontal earthquake impact coefficient can be determined from the PGA with the following formula:

$$\alpha_{max} = A_{max}\beta_{max}/1,000 , \tag{6}$$

where α_{max} is the maximum value of horizontal earthquake effect coefficient; A_{max} is the PGA; and β_{max} is the platform value of amplification factor response spectrum.

According to the measured data in the report [28], the ground motion input parameters (the PGA and the maximum value of horizontal earthquake effect coefficient) of the TMSR-LF1 plant structure under frequent earthquakes, fortification earthquakes, and rare earthquakes are shown in Table 3. Additionally, the structural story drift ratio was chosen as the engineering demand parameter (EDP) for evaluating the seismic performance of the structure [32, 33]. The corresponding parameter values for different ground motion levels are shown in Table 4.

3. Seismic Analysis under Frequent and Fortification Earthquakes

The response spectrum analysis method was employed to carry out the elastic seismic analysis of the TMSR-LF1 plant structure under frequent earthquakes and fortification earthquakes. The seismic input spectrum, shown in Figure 5, was based on the code spectrum [18]. The horizontal seismic effects in the two main directions and the torsional effects in both directions are considered in the calculation. In this section, the modal vibration patterns of the structure were analyzed, and the seismic performance of the structure under frequent earthquakes and fortification earthquakes was investigated.

3.1. Vibration Modal Analysis. The main (the first three orders) vibration models of the TMSR-LF1 plant structure model are shown in Figure 6. It can be observed that the first two order vibration modes of the structure are dominated by the translation in the X and Y directions, respectively, while the third order is dominated by the torsion, and the corresponding natural periods are basically in the range of 0.070–0.100 s. Besides, the places with large deformation are mainly concentrated in the aboveground part of the structure.

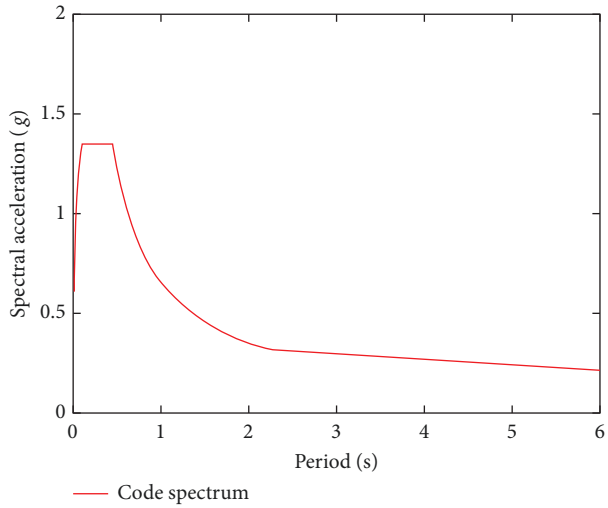

Figure 5: The seismic input spectrum.

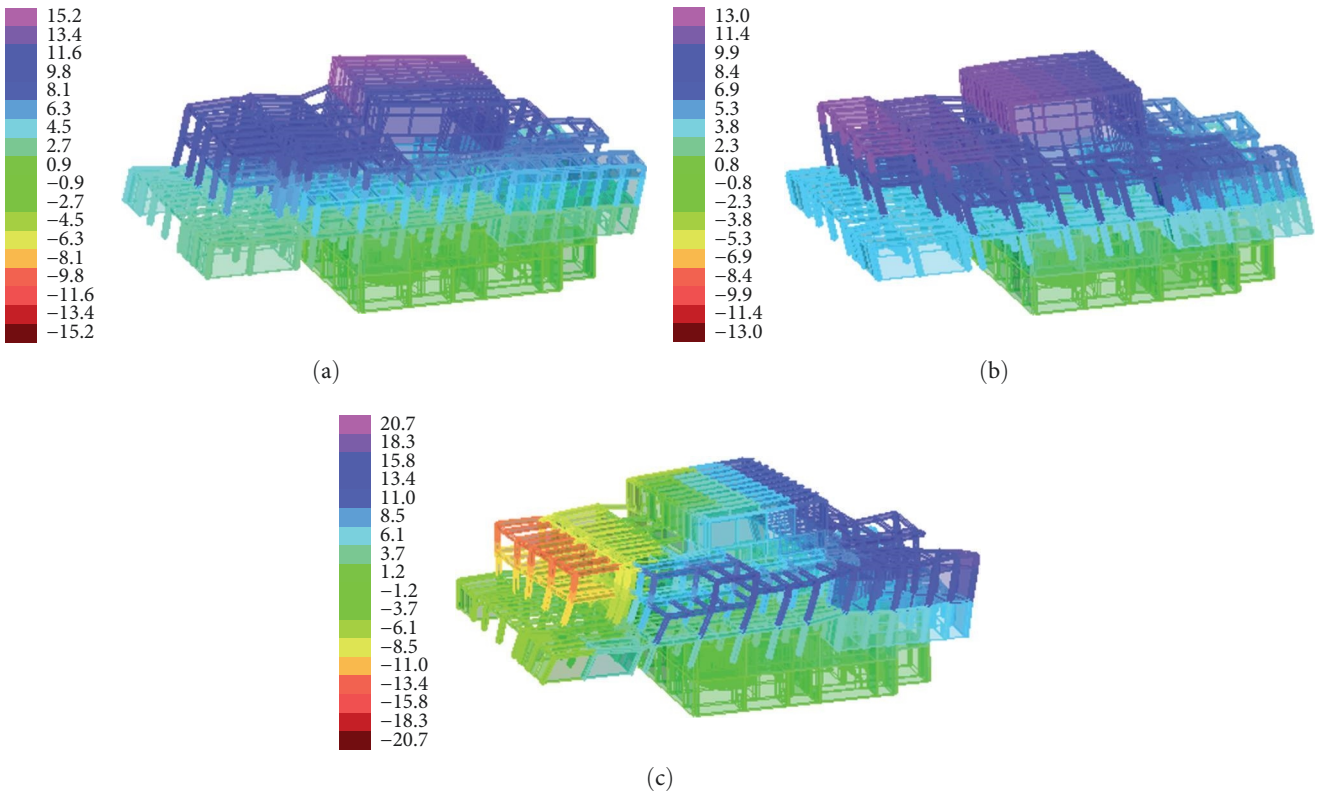

Figure 6: The main vibration modes of TMSR-LF1 structure: (a) the first order (0.093 s); (b) the second order (0.088 s); (c) the third order (0.072 s).

The number of vibration modes involved in the calculation has a large influence on the effective mass coefficient (the ratio of the mass involved in the calculated vibration modes to the total mass); in order to ensure the validity of the calculation results, eight different numbers of vibration modes (15, 20, 30, 40, 50, 60, 70, and 80) were calculated, and the corresponding variation curves of the effective mass coefficient are shown in Figure 7. It can be seen that the effective mass coefficient has exceeded 90% when the number of involved calculated vibration modes is greater than 60 [18], and the change rate is less than 0.2% after the number of calculated vibration modes continues to increase to 70.

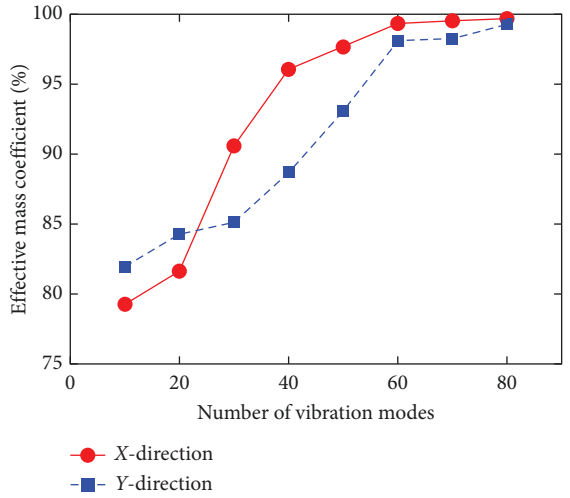

Figure 7: The variation curve of the effective mass coefficient with the number of vibration modes involved in the calculation.

Table 5: The results of the response spectrum analysis.

Parameters	X direction	Y direction	Limiting value	Evaluation
Maximum displacement ratio	1.15	1.33	<1.5	Pass
Minimum shear capacity ratio	0.96	0.96	≥0.8	Pass
Maximum story drift ratio under frequent earthquakes ($\times 10^{-3}$ rad)	0.125	0.449	<1.25	Pass
Maximum story drift ratio under fortification earthquakes ($\times 10^{-3}$ rad)	0.364	1.154	<2.50	Pass

Considering the calculation time and accuracy, the number of involved vibration modes was chosen to be 60 for the response spectrum analysis of the structural model.

3.2. Seismic Analysis under Frequent Earthquakes. The parameters for seismic performance evaluation obtained from the response spectrum analysis under frequent earthquakes are presented in Table 5 and Figure 8, which include the maximum displacement ratio, the minimum shear capacity ratio, and the maximum story drift ratio. It can be seen from Figure 8 and Table 5: (1) the maximum displacement ratio of the structure in the X and Y directions are 1.15 and 1.33, respectively, both less than 1.50, indicating that the structure plan arrangement is reasonable. Additionally, the minimum shear capacity ratio of the structure in the X and Y directions is 0.96, which is greater than 0.80, signifying that the vertical arrangement of the structure is also reasonable; (2) the maximum story drift ratio of the underground part of the structure is 0.061×10^{-3} rad, significantly smaller than the above-ground part of 0.449×10^{-3} rad, which indicates the better seismic performance of the underground part; (3) the maximum story drift ratio of the structure in X and Y directions are 0.125×10^{-3} rad and 0.449×10^{-3} rad, respectively, which are much smaller than the elastic limit of 1.25×10^{-3} rad. Overall, the above analysis results show that the structural system, structural arrangement, and component size of TMSR-LF1 are basically reasonable, and the TMSR-LF1 structure meets the fortification goal of "no damage under small earthquakes."

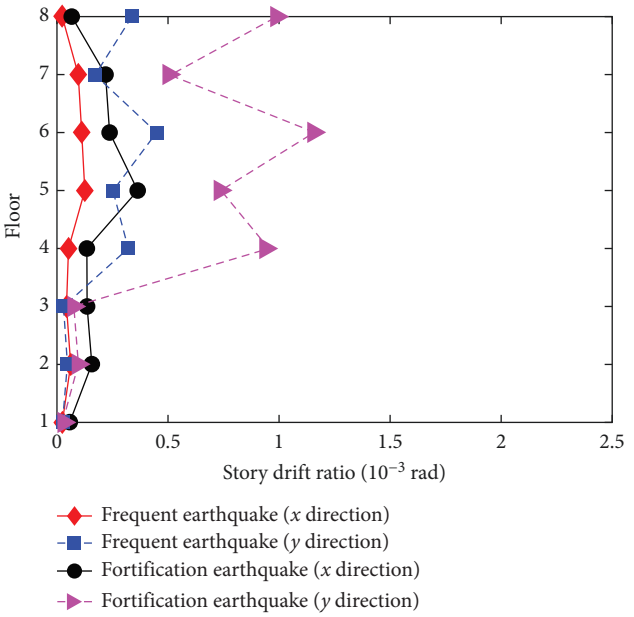

Figure 8: The story drift ratio curves by the response spectrum analysis.

3.3. Seismic Analysis under Fortification Earthquakes. The results of the story drift ratio obtained from the response spectrum analysis under the fortification earthquakes are also shown in Table 5 and Figure 8. As evidenced in Table 5 and Figure 8,

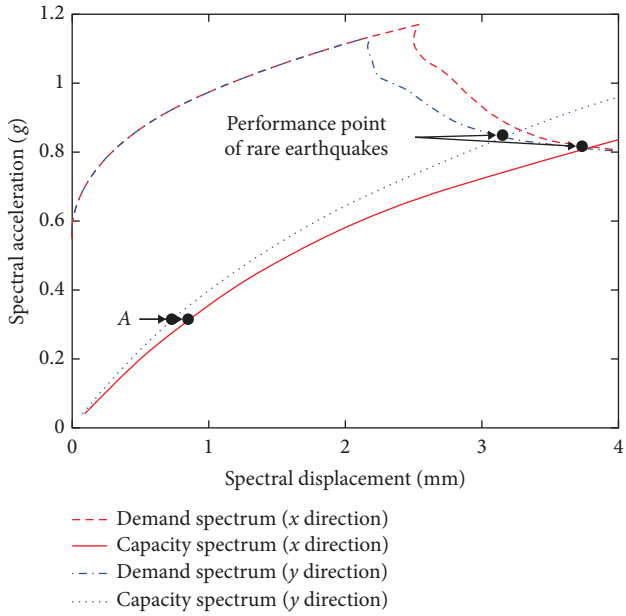

Figure 9: The pushover curves of the structure and performance points of rare earthquakes.

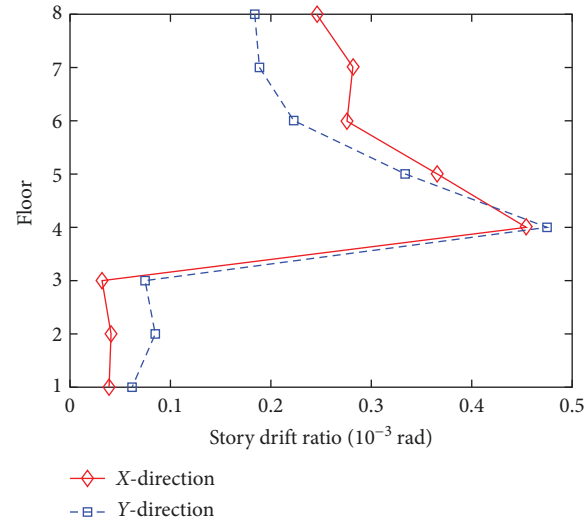

Figure 10: The story drift ratio curves of the structure by the pushover analysis.

Table 6: The maximum story drift ratio by the pushover analysis.

Direction	Maximum story drift ratio ($\times 10^{-3}$ rad)	Floor
X	0.419	4
Y	0.411	4

the story drift ratio under the fortification earthquakes follows a similar pattern to those under frequent earthquakes. Moreover, the maximum story drift ratio of the structure in X and Y directions under fortification earthquakes are 0.364×10^{-3} and 1.154×10^{-3} rad, respectively, which are 2.91 and 2.57 times greater than those under frequent earthquakes. This is because the input of the fortification earthquakes is approximately three times of the frequent earthquakes, as indicated in Table 3. It should be noted that the maximum story drift ratio is still lower than the elastic limit of 1.25×10^{-3} rad, which means that the TMSR-LF1 structure meets the fortification goal of "no unrepairable damage under medium earthquakes."

4. Seismic Analysis under Rare Earthquakes

4.1. Pushover Analysis. In this section, the stiffness performance of the structure under rare earthquakes was discussed, and seismic performance (story drift ratio) and zone damage (plastic hinge) were analyzed. The pushover analysis method was employed for the elastoplastic analysis of the TMSR-LF1 plant structure under rare earthquakes. In the calculation, the initial stress state of the structure was obtained by applying a static load in the vertical direction. Subsequently, the lateral load was incrementally applied using the arc-length method with the sum of the lateral loads equal to the total mass of the structure [34]. The pushover analysis was conducted separately in the X and Y directions using a horizontal lateral loading pattern represented an inverted triangular distribution. The structural performance point was calculated using the capacity spectrum method, which was recommended by ATC-40.

4.1.1. Stiffness Analysis. The stiffness performance of the structure significantly determines its seismic performance. Thus, to demonstrate the stiffness performance of the TMSR-LF1 plant structure, the pushover curve, including the capacity spectrum and demand spectrum curves of the structure, was given in Figure 9. It can be seen that the initial part of the capacity spectrum curve (before point A) shows a linear increase, implying that the structure is mainly in the elastic stage; the second part of the capacity spectrum curve (after point A) gradually rises, indicating that the structure has entered the plastic stage with the formation of plastic hinges. Additionally, the capacity spectrum curve does not display a falling point. It should be noted that the intersection point (performance point) of the demand spectrum and the capacity spectrum curves under rare earthquakes are located after point A, indicating that the structure is basically elastic under rare earthquakes and does not enter the yielding stage. Moreover, a comparison of the capacity spectrum curves of the structure in the X and Y directions reveals that the spectral acceleration of the structure in the Y direction is greater than that in the X direction under the same spectral displacement. Thus, the overall stiffness of the structure in the Y direction is greater than that in the X direction.

4.1.2. Seismic Performance Analysis under Rare Earthquakes. The story drift ratio curves and their maximum value obtained from the pushover analysis under rare earthquakes are shown in Figure 10 and Table 6. It is clear that the story drift ratio of the TMSR-LF1 plant varies by direction and by location within the structure. The underground portion of the plant has a larger story drift ratio in the Y direction (0.085×10^{-3} rad) than in the X direction (0.041×10^{-3} rad), while the aboveground portion has a larger story drift ratio in the X direction (0.419×10^{-3} rad) than in the Y direction (0.411×10^{-3} rad).

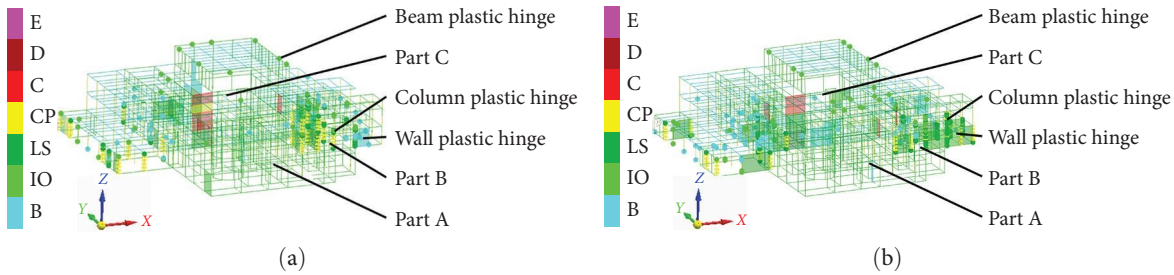

Figure 11: The plastic hinge of the structure by the pushover analysis under rare earthquakes: (a) X direction; (b) Y direction.

In addition, the curves of the story drift ratio of the structure present a similar trend in the X and Y directions, and the maximum values both appear on the 4th floor. Importantly, both of these two maximum values are much smaller (0.419×10^{-3} rad in the X direction and 0.411×10^{-3} rad in the Y direction) than the collapse limit of 10×10^{-3} rad [18], suggesting that the TMSR-LF1 structure can withstand rare earthquakes without collapsing. Overall, these results demonstrate that the TMSR-LF1 plant meets the fortification goal of "no collapse under rare earthquakes."

4.1.3. Zone Damage Analysis. The distribution and extent of the plastic hinge of the structure obtained from the pushover analysis under rare earthquakes are presented in Figure 11. The legend in Figure 11 is shown from bottom to top as B: yield; IO: any repairs are minor; LS: structure remains stable and has significant reserve capacity; CP: collapse prevention; C: ultimate bearing capacity; D: residual strength of pushover analysis; E: total failure.

The results indicate that the structural integrity of Part A remains primarily elastic, especially the reactor system and reactor surround system area, which are completely in the elastic range. Most of the components in Part B demonstrate elastic deformation, while the plastic hinges tend to concentrate on columns and shear walls. Moreover, the number and extent of the plastic hinges observed in columns and beams gradually decrease as the floor rises. The analysis of Part C reveals that the distribution and extent of plastic hinges are similar to those observed in Part B. However, this part comprises relatively more plastic hinges and experiences deeper plastic deformations.

4.2. Elastoplastic Time History Analysis. The elastoplastic time history analysis method was applied to the analysis of the TMSR-LF1 plant structure under rare earthquakes. To sufficiently consider the effects of the two-directional principal components of each seismic wave set, the seismic principal components were input in the X and Y directions of the structure, respectively. Furthermore, a three-directional seismic wave input was utilized to a conservative estimation. The accelerations in the horizontal primary, horizontal secondary, and vertical directions were input at peak accelerations of 0.46, 0.391, and 0.299 g, respectively, and in proportion to the scale factor of 1.00 : 0.85 : 0.65, as seen in Table 3 (g is the acceleration of gravity, $g = 9.8\ \mathrm{m/s^{-2}}$). In this section, the selection of seismic waves was discussed, and in combination with Section 4.1, the structural response results obtained from the pushover analysis and the elastoplastic time history analysis were compared and analyzed, and then the conservativeness of the two methods was reviewed.

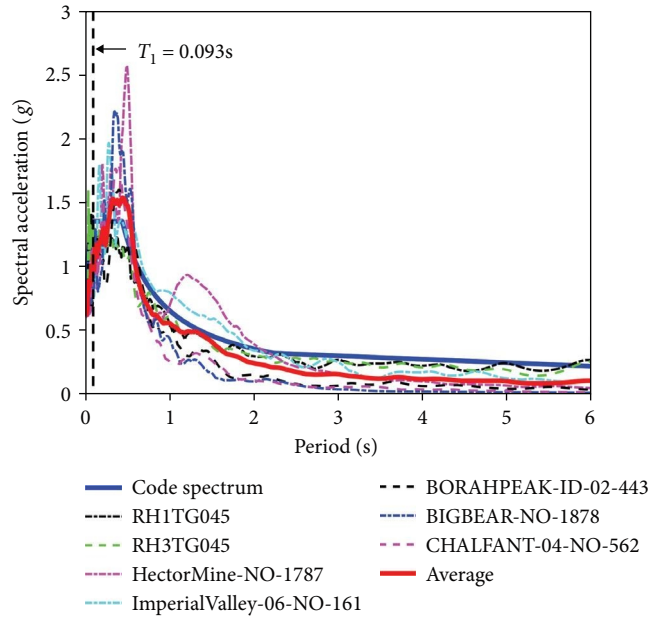

Figure 12: Spectral curves of the chosen seismic waves and code.

4.2.1. Seismic Wave Selection. In the elastoplastic time history analysis of the structure, the seismic waves at the actual site were difficult to obtain. Therefore, the code spectrum [18] was used as the target spectrum in this study. A total of seven sets of seismic waves commonly used in engineering were selected from the PKPM Ground Motion Database. These seismic waves, including five sets of natural seismic waves (HectorMine-No-1787, ImperialValley-06-No-161, BORAHPEAK-Id-02-443, BIGBEAR-No-1878, and CHALFANT-04-No-562) and two sets of artificial waves (RH1TG045 and RH3TG045). The natural seismic waves accounted for 71% of the total waves selected, meeting the rule of 2/3. Figure 12 shows the acceleration response spectrum curves of seven sets of seismic waves at the damping ratio of 0.05. It can be seen that the selected seismic waves have similar characteristics as the code response spectrum (GB50011 spectrum). Additionally, the error δ between the code spectrum value and the average response spectrum value (1.15 g) obtained from the time history analysis is 13.3%, which is not greater than 20%,

Table 7: Comparison results of the base shear force.

Analysis method	X (KN)	Ratio (%)	Y (KN)	Ratio (%)	Limit value (%)
Code spectrum analysis	40,253	—	39,392	—	—
Time history analysis					
Minimum value	39,236	97	38,596	97	> 65
Maximum value	51,910	129	48,931	124	<135
Average values	44,283	110	42,163	107	> 80 and <120

Table 8: The structural damage state under seven sets of seismic waves by the elastoplastic time history analysis.

Seismic waves	Damage state
RH1TG045	Collapse
RH3TG045	Collapse
HectorMine-NO-1787	Collapse
ImperialValley-06-NO-161	Collapse
BORAHPEAK-ID-02-443	Noncollapse
BIGBEAR-NO-1878	Noncollapse
CHALFANT-04-NO-562	Noncollapse

at the period T1 (0.093 s) of the main vibration mode (1st order vibration mode) of the structure. Table 7 displays the structural base shear results obtained from both code spectrum and time history analysis. It can be seen that the minimum value derived from the selected time history calculation is greater than 65% of the code spectrum result, while the maximum value is less than 135% of the code spectrum results, and the average value falls within the range of 80% and 120% of the code spectrum results. Based on the above analysis, it is shown that the chosen seismic waves satisfy the requirements of the specification and can be used for subsequent analysis.

4.2.2. Conservative Analysis. The results of the structural damage state (collapse/noncollapse) obtained from the elastoplastic time history analysis under seven sets of seismic waves are shown in Table 8. It can be seen from Table 8 that the structure collapsed under the action of two sets of artificial waves (RH1TG045 and RH3TG045) and two sets of natural seismic waves (HectorMine-NO-1787 and Imperial-Valley-06-No-161), with a collapse rate reached 57.14% (number of waves collapsed/total number of waves).

Figure 13 and Table 9 show the results of the structural story drift ratio under the action of three sets of seismic waves (BORAHPEAK-ID-02-443, BIGBEAR-NO-1878, and CHALFANT-04-NO-562) that are not leading to the structure collapse. The presented Figure 13 and Table 9 depict that the results of structure story drift ratios, analyzed by the uncollapsed three sets of seismic waves, are much larger than the results of pushover analysis, and the maximum values of the story drift ratios in the X and Y directions are 3.424×10^{-3} and 3.571×10^{-3} rad, respectively. These values are 8.17 and 8.69 times greater than the pushover analysis results (0.419×10^{-3} and 0.411×10^{-3} rad). In addition, it can be seen from Figure 13 that the story drift ratio curves for the three sets of seismic waves are more significantly different in the X direction compared to the Y direction. This is influenced by the dynamic properties of the structure and the spectral properties of the input seismic waves. The first-order (T1) and second-order (T2) vibration modes of the structure are shown in Figure 6 to be translational in the X and Y directions, respectively. The response spectral values at the T1 and T2 periods are provided in Table 10. The differences in the response spectral values are large at the T1 period, which are 0.7632, 0.7830, and 0.8997 g, respectively (their ratio is 1.00 : 1.02 : 1.18), while the differences are small at the T2 period, which are 0.8017, 0.7322, and 0.8639 g, respectively (their ratio is 1.00 : 0.91 : 1.08).

Based on the relatively large result of the story drift ratio of the structure under the action of the natural seismic wave CHALFANT-04-NO-562 (see Table 9), the damage of the structural zone under the action of this wave has been analyzed. To further understand the plastic hinge distribution and plastic hinge ratio of the beam and column components, Figure 14 and Table 11 have been included in the analysis. It can be seen that Part A of the structure has high stiffness and thus showed mostly elastic behavior, which is consistent with the results of the pushover analysis. In Parts B and C of the structure, however, the number of plastic hinges increased significantly in the elastoplastic time history analysis compared to the pushover analysis. The maximum hinge rates of the beams and columns in the X and Y directions were observed to be 6.53% and 50.45%, respectively, which are 1.87 and 1.54 times higher than the former (3.50% and 32.68%).

Through the above analysis, it can be observed that the elastoplastic time history analysis exhibits greater conservatism compared to the pushover analysis.

4.3. Structural Reinforcement Analysis. The previous analysis revealed that the TMSR-LF1 plant structure cannot meet the seismic design goal of "no collapse in large earthquakes" during seismic analysis by the elastoplastic time history analysis. Therefore, adequate reinforcement [27, 35, 36] is imperative. Since the damage of the structure mainly occurs in the aboveground part, the following three measures have been recommended to enhance and reinforce the structure components above +0 m elevation: (1) the column cross-sectional size of the structure will be upgraded from 600 mm × 600 mm to 800 mm × 800 mm; (2) the infill wall and shear wall components on both sides of the exterior wall and aisle of the structure will be modified to shear walls with an 800 mm thickness; (3) the infill wall elements in

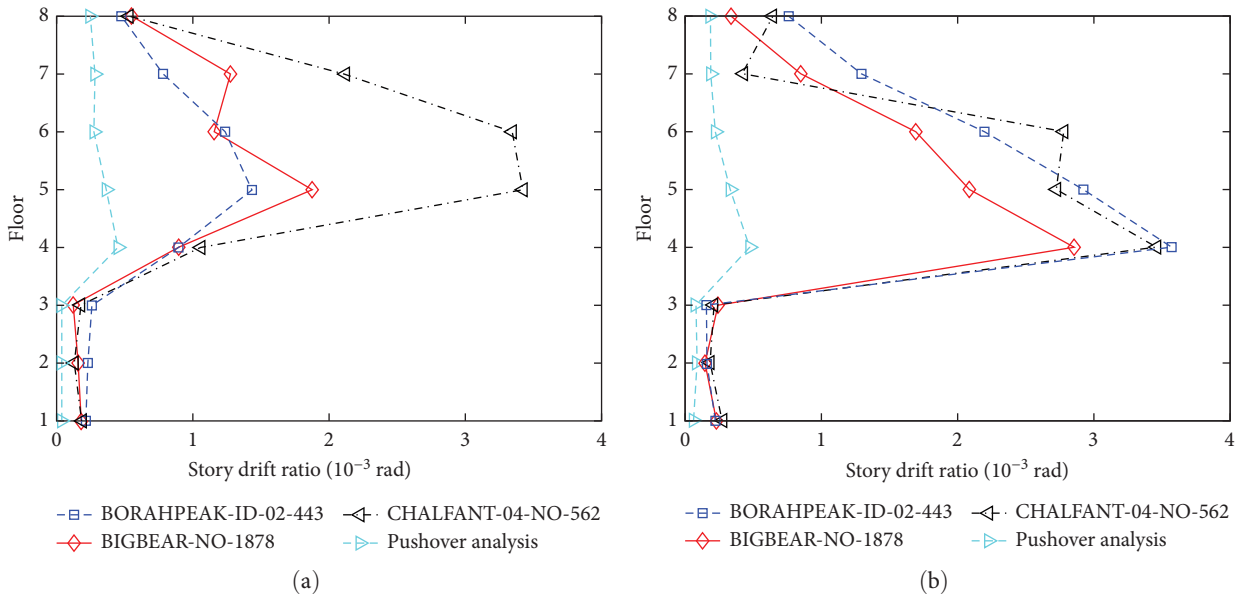

Figure 13: Comparison of the story drift ratio curve under rare earthquakes: (a) X direction; (b) Y direction.

Table 9: Comparison of maximum story drift ratios of the structure under rare earthquakes.

Seismic waves	Direction	Maximum story drift ratio ($\times 10^{-3}$ rad)
BORAHPEAK-ID-02-443	X	1.434
	Y	3.571
BIGBEAR-NO-1878	X	1.876
	Y	2.857
CHALFANT-04-NO-562	X	3.424
	Y	3.460
Pushover analysis	X	0.419
	Y	0.411

Table 10: Comparison of response spectral values (g) of different seismic waves at the T1 and T2 vibration periods of TMSR-LF1.

Seismic waves	BORAHPEAK-ID-02-443	BIGBEAR-NO-1878	CHALFANT-04-NO-562
T1 (X)	0.7632	0.7830	0.8997
T2 (Y)	0.8017	0.7322	0.8639

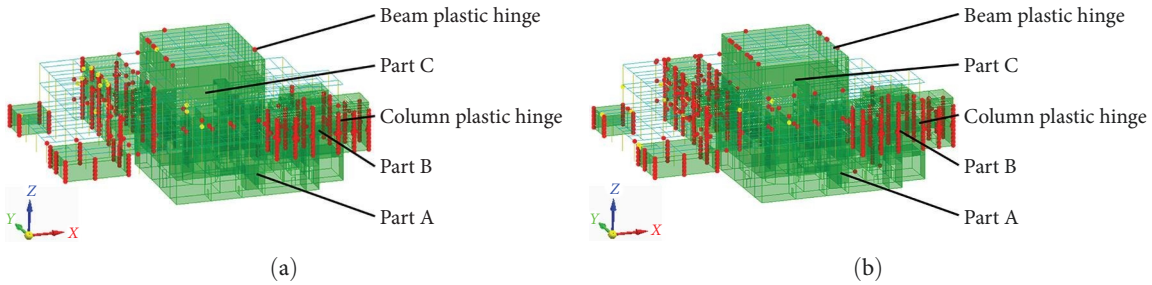

Figure 14: The plastic hinge of the structure by the elastoplastic time history analysis under rare earthquakes: (a) X direction; (b) Y direction.

Table 11: Comparison of plastic hinge ratio of the structure by the elastoplastic time history analysis under rare earthquakes.

Analysis method	Direction	Plastic hinge ratio (%)		Ratio	
		Beam	Column	Beam	Column
Elastoplastic time history analysis	X	6.53	50.45	1.87	1.54
	Y	4.22	43.22	1.46	1.35
Pushover analysis	X	3.50	32.68	1.00	1.00
	Y	2.90	31.92	1.00	1.00

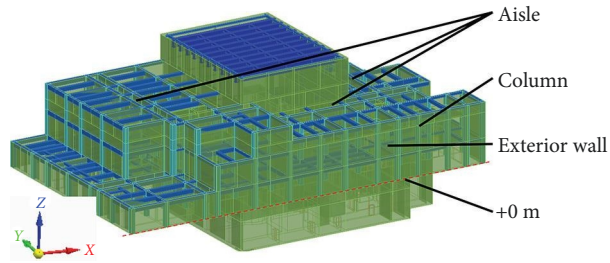

Figure 15: The 3D model of the reinforced TMSR-LF1 plant structure.

Table 12: Comparison of different seismic wave calculations results for the original structure and reinforced structure.

Seismic waves	Collapse (—)/non-collapse (maximum story drift ratio ($\times 10^{-3}$ rad))	
	Original structure	Reinforced structure
RH1TG045	Collapse (—)	Noncollapse (0.822)
RH3TG045	Collapse (—)	Noncollapse (1.002)
HectorMine-NO-1787	Collapse (—)	Noncollapse (0.507)
ImperialValley-06-NO-161	Collapse (—)	Noncollapse (0.452)
BORAHPEAK-ID-02-443	Noncollapse (3.571)	Noncollapse (0.274)
BIGBEAR-NO-1878	Noncollapse (2.857)	Noncollapse (0.352)
CHALFANT-04-NO-562	Noncollapse (3.460)	Noncollapse (0.128)

other areas of the structure will be replaced with shear walls with a thickness of 400 mm. Figure 15 presents a 3D model of the reinforced TMSR-LF1 plant structure.

The seismic analysis of the reinforced structure was conducted under the same input conditions as in Section 4.2. Table 12 illustrates the damage states and the maximum story drift ratios of both the original structure and the reinforced structure under different seismic waves. The results reveal that the reinforced structure exhibited no signs of collapse under any seismic waves. Additionally, the maximum story drift ratio of the reinforced structure was only 1.002×10^{-3} rad, which was much smaller than the maximum value of the original structure in the case of no collapse (3.571×10^{-3} rad). The above results indicate that the reinforcement measures effectively improved the seismic performance of the TMSR-LF1 plant structure and made the structure meet the seismic design goal of "no collapse under rare earthquakes" during the elastoplastic time history analysis.

5. Conclusion

The seismic performance analysis of the TMSR-LF1 plant structure was carried out using the finite element software PKPM and the seismic design method of the civil code +1°. The analysis was performed under the action of frequent earthquakes, fortification earthquakes, and rare earthquakes. The conservatism of the pushover analysis and the elastoplastic time history analysis methods were also discussed. Additionally, a reinforcement of the structure analysis was performed. Several conclusions were obtained as follows:

(1) The response spectrum analysis under frequent and fortification earthquakes shows that the TMSR-LF1 plant has the capability to bear seismic waves, meeting the seismic design goals of "no damage from small earthquakes" and "no unrepairable damage under medium earthquakes."

(2) The pushover analysis under rare earthquakes demonstrated that the maximum story drift ratio of the structure is far below the code limit. Further, the core area where critical system equipment is located remains entirely in the elastic range. These findings suggest that the TMSR-LF1 plant can meet the seismic design goal of "no collapse under rare earthquakes."

(3) In comparison to the pushover analysis, the seismic response (the story drift ratio and plastic hinge of structure) of the elastoplastic time history analysis

is significantly increased, indicating that it has better conservatism. Consequently, adopting the elastoplastic method for analyzing rare earthquakes is recommended for Class II research reactor plants in the future. Furthermore, to meet the seismic design goal of "no collapse under rare earthquakes" during the elastoplastic time history analysis, appropriate structural reinforcement should be used for the TMSR-LF1 plant structure.

This paper aims to examine the conservatism of the pushover analysis method and the elastoplastic time history analysis method in seismic calculations, specifically in the context of the TMSR-LF1 plant. By conducting a seismic performance analysis of this plant, the study provides valuable insights and findings that can be applied to similar Class II research reactor plants. The research findings in this paper offer a valuable reference for analyzing the seismic performance of other plants in this category.

Data Availability

The authors confirm that the data supporting the findings of this study are available within the article.

Conflicts of Interest

The authors declare that they have no known competing financial interests or personal relationships that could have appeared to influence the work reported in this paper.

Acknowledgments

The authors express their gratitude to the "Strategic Priority Research Program" of the Chinese Academy of Sciences (grant no. XDA02010000) for the financial support of this research.

References

[1] Ministry of Ecology and Environment of the People's Republic of China, "Safety licensing procedures for nuclear power plants, research reactors and nuclear fuel cycle facilities," 2019.

[2] X. Zhu, R. Pan, J. Zhu, and O. Zhang, "Comparison analysis of design seismic response spectrum used in the design of research reactor facility," *Technology for Earthquake Disaster Prevention*, vol. 13, no. 4, pp. 822–828, 2018.

[3] Y. Liu, X. Wang, X. Wang, X. Zhang, W. Gong, and R. Dai, "Floor response spectra analysis of a nuclear reactor considering uncertainties in soil parameters," *Structures*, vol. 37, pp. 305–317, 2022.

[4] X.-W. Lyu, X.-B. Xia, Z.-H. Zhang, J. Cai, and C.-Q. Chen, "Analysis of tritium production in a 2 MW liquid-fueled molten salt experimental reactor and its environmental impact," *Nuclear Science and Techniques*, vol. 27, no. 4, pp. 7–13, 2016.

[5] M. Wu, N. Zhang, J. Zhai, G.-Y. Zhou, and S.-T. Tu, "CFD studies on the separation performance of a new combined gas–solid separator used in TMSR-SF," *Nuclear Science and Techniques*, vol. 30, no. 9, pp. 106–117, 2019.

[6] Y. Liu, X. Wang, X. Wang, H. Fan, and X. Zhang, "Analysis of floor response spectra of TMSR-LF1 considering soil–structure interaction," *Nuclear Science and Techniques*, vol. 44, no. 7, pp. 85–92, 2021.

[7] M. Bayat, M. Bayat, and M. Bayat, "An analytical approach on a mass grounded by linear and nonlinear springs in series," *International Journal of Physical Sciences*, vol. 6, no. 2, pp. 229–236, 2011.

[8] M. Bayat, M. Shahidi, and M. Bayat, "Application of iteration perturbation method for nonlinear oscillators with discontinuities," *International Journal of Physical Sciences*, vol. 6, no. 15, 2011.

[9] M. Bayat, M. Shahidi, A. Barari, and G. Domairry, "Analytical evaluation of the nonlinear vibration of coupled oscillator systems," *Zeitschrift für Naturforschung A*, vol. 66, no. 1-2, pp. 67–74, 2011.

[10] Z. Xue, Y. Peng, Q. Pei, K. Zhu, and Y. Zhang, "Pushover research of reactor building structure," *Journal of Dalian University*, vol. 39, no. 6, pp. 15–18 23, 2018.

[11] Y. Qi and H. Wan, "The capacity of resisting collapse of the main power building gable nearby nuclear island," *Southern Energy Construction*, vol. 1, no. 1, pp. 70–74, 2014.

[12] J. Zhao, Y. Jin, and G. Wang, "Structural dynamic antiseismic performance analysis on the main machine hall in conventional island of Tianwan nuclear power station unit 5, 6," *Earthquake Resistant Engineering and Retrofitting*, vol. 36, no. 6, pp. 88–94, 2014.

[13] R. Pan, H. Luan, X. Zhu, and C. Hou, "Static elastoplastic response analysis of nuclear island building under excess design basis earthquake," *Industrial Construction*, vol. 46, no. 10, pp. 13–16, 2016.

[14] Y. Zhao and X. Zhang, "Seismic performance evaluation of nuclear waste plants based on pushover method," *Industrial & Science Tribune*, vol. 16, no. 15, pp. 46-47, 2017.

[15] X. Wang, D. Lu, and G. Hou, "Shaking table tests and numerical simulation analysis of a 1:15 scale model reinforced concrete containment vessel," in *21st International Conference on Nuclear Engineering*, vol. 2, Nuclear Engineering Division, 2013.

[16] X. Wang, G. Hou, and D. Lu, "Shaking table tests of a 1:15 reinforced concrete containment vessel model for a nuclear power plant," *Engineering Mechanics*, vol. 31, no. S1, pp. 249–252, 2014.

[17] B. Farmanbordar, A. B. Adnan, M. M. Tahir, and I. Faridmehr, "Seismic assessment of base-isolated nuclear power plants," *Advances in Computational Design*, vol. 2, no. 3, pp. 211–223, 2017.

[18] GB50011-2010, *Code for Seismic Design of Buildings*, China Architecture & Building Press, 2010.

[19] R. Pan, "Design seismic response spectrum used in the design of nuclear facilities other than NPPs," *Nuclear Safety*, vol. 3, pp. 36–41, 2010.

[20] Y. Liu, X. Wang, X. Wang, X. Zhang, W. Gong, and R. Dai, "Study on seismic design method of Class II research reactor based on TMSR-LF1," *Nuclear Power Engineering*, vol. 43, no. 5, pp. 223–228, 2022.

[21] X. Zhang, W. Liu, H. Ren, S. Yang, Y. Li, and X. Liu, "Structural analysis of a concrete supertall buildings," *IOP Conference Series: Earth and Environmental Science*, vol. 510, no. 5, Article ID 052008, 2020.

[22] G. Yang, T. Shi, Z. Wei, and Y. Zhou, "Research on period reduction factor of frame structure with filled wall," *Building Science*, vol. 36, no. 5, pp. 39–45, 2020.

[23] JGJ 94-2008, *Technical Code for Building Pile Foundations*, China Architecture & Building Press, 2008.

[24] L. Tulin and K. Gerstle, "Discussion of equation for the stress-strain curve of concrete-by Desayi and Krishnan," 1964.

[25] M. Faiz and R. Kumar, "Comparative effectiveness of equivalent static analysis & response spectrum analysis in extreme seismic zones," *IOP Conference Series: Earth and Environmental Science*, vol. 1110, no. 1, Article ID 012013, 2023.

[26] F. Barbagallo, M. Di Domenico, M. Terrenzi et al., "Influence of the modelling approach on the seismic assessment of RC structures by nonlinear static analyses," *Soil Dynamics and Earthquake Engineering*, vol. 172, Article ID 107970, 2023.

[27] F. Wang, Q.-X. Shi, and P. Wang, "Seismic behaviour of reinforced concrete frame structures with all steel assembled Q195 low yield buckling restrained braces," *Structures*, vol. 30, pp. 756–773, 2021.

[28] F. Xie, *Seismic Safety Evaluation Report on Site Selection Project of TMSR Advanced Nuclear Experimental Base*, Institute of Geology, China Earthquake Administration, Beijing, 2017.

[29] M. Niloufar, K. Ali, and Z.-H. Rouzbeh, "Dynamic increase factor for investigation of progressive collapse potential in tall tube-type buildings," *Journal of Performance of Constructed Facilities*, vol. 30, no. 6, 2016.

[30] B. D. Zhao, Y. Chen, C. Q. Liu, H. D. Wu, T. Wang, and X. D. Wei, "An axial semi-rigid connection model for cross-type transverse branch plate-to-CHS joints," *Engineering Structures*, vol. 181, pp. 413–426, 2019.

[31] Y. Ma, Z. Wu, Z. Liu, M. Zhang, and M. Aibaidula, "Seismic fragility analysis of aqueduct structural systems based on G-PCM method," *Sustainability*, vol. 14, no. 20, Article ID 13161, 2022.

[32] C. Liu, D. Fang, and Z. Yan, "Seismic fragility analysis of base isolated structure subjected to near-fault ground motions," *Periodica Polytechnica-Civil Engineering*, vol. 65, no. 3, 2020.

[33] J. Zhang, *Study on the Application of Ground Motion Intensity Measures in the Seismic Analysis of Hydropower House*, Xi'an University of Technology, 2020.

[34] China Academy of Architectural Engineering, "PUSH&EPDA elastoplastic static and dynamic analysis software for multi-storey and high-rise structures (V3.1) user's manual," 2010.

[35] Z. Tang, Z. Peng, and X. Liu, "Numerical study on optimal design and seismic capacity of double-span RC frame structures with exterior verandahs," *Buildings*, vol. 12, no. 11, Article ID 1901, 2022.

[36] H. Han, *Research on Effect of Shear Wall Thickness Variation on Seismic Performance of Shaft Tower Structure*, Xi'an University of Science and Technology, 2014.